The final publication is available at

https://doi.org/10.1177/1468087420921584

Additional Information

A one-dimensional modelling study on the effect of advanced insulation coatings on ICE efficiency

Alberto Broatch, Pablo Olmeda, Xandra Margot and Josep Gomez-Soriano[*]

CMT - Motores Térmicos, Universitat Politècnica de València, Camino de Vera s/n, 46022 Valencia, Spain

Corresponding author (*):
Josep Gomez-Soriano PhD. (jogoso1@mot.upv.es)
Phone: +34 963 877 650
Fax: +34 963 877 659

Abstract

The present paper presents a study of the impact on engine efficiency of the heat loss reduction due to in-cylinder coating insulation. A numerical methodology based on 1D Heat Transfer Model (HTM) is developed. Since there is no analytic solution for engines, the 1D model was validated with the results of a simple 'equivalent' problem, and then applied to different engine boundary conditions. Later on, the analysis of the effect of different coating properties on the heat transfer using the simplified 1D HTM is performed. After that, the model is coupled with a complete virtual engine that includes both thermodynamic and thermal modeling. Next, the thermal flows across the cylinder parts coated with the insulation material (piston and cylinder head) are predicted and the effect of the coating on engine indicated efficiency is analyzed in detail. Results show the gain limits, in terms of engine efficiency, that may be obtained with advanced coating solutions.

Keywords

1D thermal modelling, insulation coatings, heat transfer, engine efficiency

1. Introduction

The number of actions for searching an inclusive and sustainable solution for transport-related issues has significantly increased in recent years, and have become a topic of current interest in all society collectives[1]. Particularly, the investigation for cleaner and more efficient Internal Combustion Engines (ICEs) is nowadays the main objective of all engine manufacturers (OEMs), since they represent nearly 26% of the total CO_2 emissions. The development of current

---

[1] In this context, the Paris climate conference (COP21), the United Nations Conference on sustainable Development (Rio + 20) or Horizon 2020 are such examples of administrative measures to deal with the actual paradigm.

engines is being directed following two different paths, which in most cases are opposed. For example, the increased levels of nitrogen oxides (NO_x) linked to an enhanced combustion process goes against the improving thermal efficiency achieved. Therefore, the search of higher efficiency levels to reduce to the minimum the amount of CO_2 emitted per unit of fuel consumed are usually contrary to the air quality improvement due to the pollutant emissions reduction (i.e. particulate matter, carbon monoxide, NO_x, etc.), especially in urban environments where the number of respiratory diseases has significantly grown owing to these.

The struggle between these developing lines is leading to increased efforts for enhancing ICE performance to radically reduce the impact on our environment. To name but the most relevant: increasing the compression ratio [1], lean combustion concepts [2][3][4] or new fuels/additives [5][6].

Reducing the heat transfer (HT) through the chamber walls is still a hot topic today [7][8][9]. For instance, the adiabatic by part approach consists in insulating internal parts, specially the piston head, cylinder head and valves, if possible to decrease thermal losses but also the exhaust manifold in order to maintain the highest admissible temperature for turbine inlet. In this way, higher brake power may be achieved.

The use of ceramic insulation coatings brings about a notable HT decrease that may lead to an enhanced cycle efficiency [10]. However, the negative heat flow (heat from walls to the gas) heats up the intake gases during the exchange process, resulting in a significant deterioration of the volumetric efficiency that affects the brake power [11]. However, other authors [12][13] claim that advanced insulation coatings mimic the gas temperature swing during the engine cycle [14][15][16]. This fact allows reducing thermal losses during combustion, while keeping the surface temperature during the exchange process low enough to maintain the volumetric efficiency [17].

Several works related to this topic were conducted by *Toyota Central R&D Labs Inc.* considering both spark-ignition and compression-ignition diesel engines [13][17][18][19]. They published results proving that materials with low conductivity and thermal capacitance applied solely to the piston surface can reduce HT during combustion, consequently improving the thermal efficiency of the engine in a significant way. However, some of the conclusions of these works differ from most of the investigations carried out to date: from Heywoods's classical work [20] to more recent studies performed by Rakopoulos et al. [21] and Chang et al. [22] –whom have used thermocouple-based techniques– and Kikusato et al. [23] through numerical simulations. In these works, the maximum wall temperature swing, and thus the reduction in HT, are remarkably lower than the values claimed by *Toyota*.

Some of *Toyota's* results are justified and validated with wall temperature measurements made with the Laser-Induced Phosphorescence (LIP) technique. Since this method is based on emission processes that follow after the absorption of light, the surface temperature measurement is taken at a given point located on the surface of interest (piston, cylinder head, etc) with the help of a laser beam. This means that the surface temperature swing can differ notably if the thermodynamic processes on the gas side have remarkable spatial differences. This is critical in compression-ignition (CI) diesel engines where the surface temperature swing is substantially higher at a point of spray impingement than in other areas of the combustion chamber [13] (i.e. in the squish region). In spark-ignition (SI) engines, though less pronounced, this effect can be also relevant since the temperature differences between the centre and the

periphery of the piston can be significant [26]. Due to these reasons, there are some concerns about whether these measurements are sufficiently representative to estimate the HT flow during the engine operation.

In addition, Knappe et al. [24] demonstrated that the results obtained with LIP depend highly on the thickness of the phosphor, which in fact produces an insulating effect due to its low conductivity. Since it is extremely difficult to control the phosphor thickness when applying it, and even more so during combustion, as the phosphor layer is depleted during the process, the reliability of this technique seems questionable. This is corroborated by Algotson et al. [25] who show that due to the insulating effect of the phosphor coating, wall temperatures are systematically overestimated when compared with thermocouple measurements and simulation results. Despite these limitations, the LIP technique is very interesting from the point of view of the materials engineering. It can provide raw measurements of local temperatures, useful for the estimation of thermal stresses and material strengths.

The objective of this paper is therefore to develop a computational tool, referred as 1D Heat Transfer Model (HTM), for the assessment of the heat losses in the combustion system with coating insulation. The main idea is to understand the physics of heat losses through the combustion chamber walls coated with different materials, taking into account important factors, such as the material properties and/or geometric features. Although the basis of this method is not new (similar approaches have been published in the past [27]), none of the published works account for the impact of different materials and geometrical properties. In this sense, the novelty of this approach lies in the study of the suitability of applying different advanced coatings on in-cylinder parts in order to reduce the heat losses and to quantify the impact of this technology on the increase of the engine thermal efficiency. The methodology is set up using data from a Direct Injection (DI) compression-ignition diesel engine.

In the following section of this paper, the theoretical background, the 1D HTM model definition and the calculation methodology are presented. Section 3 is dedicated to the analysis of the effect of different coating properties on the heat transfer using the simplified 1D HTM described in section 2. A trade-off between the heat insulation and the negative heat for different coating materials and thicknesses is identified. Moreover, the thermal flows through the insulated cylinder parts are predicted and the effect of the coating on engine indicated efficiency is analysed in detail. Finally, the main conclusions obtained from the results are drawn in section 4.

2. Materials and methods

This section describes the theoretical background used as basis for evaluating the heat losses reduction achieved when using coating on some parts of the internal walls of an engine combustion chamber. After de 1D HTM model description, a validation procedure based on the analytical solution of a problem with similar characteristics to those occurring in an engine is presented. Finally, the 1D HTM was coupled with a virtual engine model to estimate the impact of the HT reduction on the engine thermal efficiency.
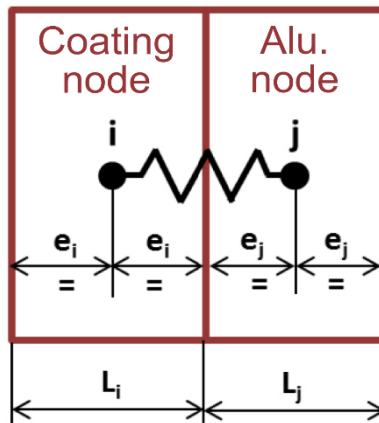
2.1. Numerical model

A numerical 1D lumped model of the solid has been developed on the basis of the lumped capacitance approach used in engine-related applications [32]. It computes the heat flux of simplified solid with transient boundary conditions (BC) in the gas side (both temperature and heat transfer coefficient varying with the time). The lumped model reduces the combustion

chamber thermal system (in this case the piston, cylinder head, the liner and the bottom of the valves) to a discrete number of nodes assuming constant temperature for each of them. This geometry simplification of the combustion chamber surface elements in discrete nodes implies that the radial temperature distribution in a cross sectional area is negligible compared to the axial one.

In order to account for different materials, the interface between the coating and the substrate (aluminum) can be modeled assuming two conductances connected in series. The equation for conductive conductance corresponds to a one dimensional case of conduction between two adjacent planes of different materials (*Figure 1* and Eq. 8).

$$K_{ij} = \frac{k_i k_j}{e_i k_j + e_j k_i} \cdot A_{ij} \qquad \text{Eq. 8}$$

In this equation, k_i and k_j are the conductive conductances of the coating and the aluminum, respectively. The distance between the planes (e_i and e_j) and the contact areas (A_{ij}) are geometric parameters directly obtained by measurements and/or some assumptions described in the following sections.

Figure 1: Schematic of the modeling approach for the interface of two different materials.

The numerical solution is obtained by iterating, while the steady solution of each node (solving the problem with the time-averaged temperature and heat transfer coefficient as constant BCs) was used as initial conditions for the transient simulation to reduce the computational time. The number of nodes was chosen after an independence study and it resulted on 20 nodes for the coating material and 50 for the aluminum material.

2.1.1. Application to engine boundary conditions

The numerical model has been used to simulate the insulation performance of coated surfaces at real-engine operating conditions. Several boundary conditions must be considered for the calculation of the instantaneous heat transfer through a solid surface considering the following aspects:

- The heat transfer through the solid is three dimensional.

- On one side of the solid (in-cylinder combustion chamber), both the heat transfer coefficient (h) and the gas temperature (T_g) vary with time during a thermodynamic cycle.
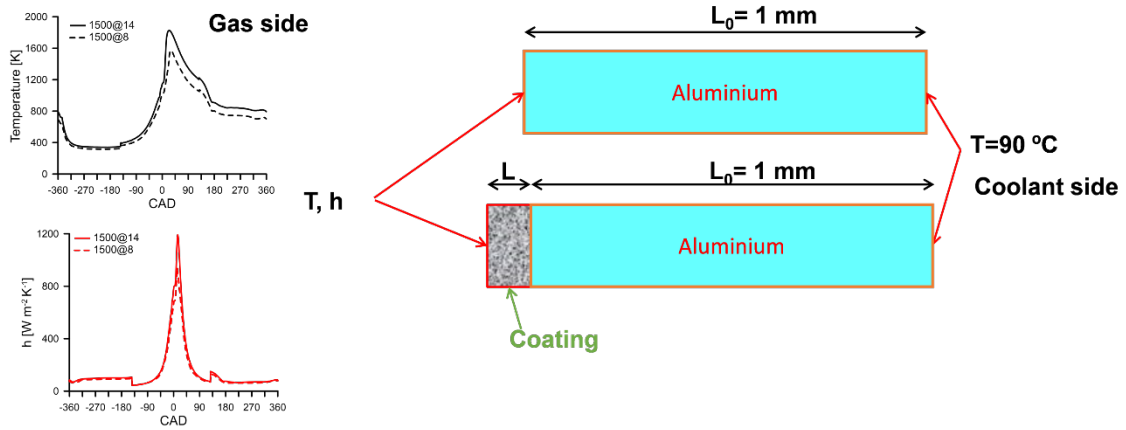
- On the other side (oil/coolant side), both the heat transfer from walls to the oil and the coolant temperature can be assumed to be constant with time during a thermodynamic cycle.

The simple geometry of a solid bar has been considered, as shown in *Figure 2* and the following lengths have been used for calculations:

- 1 mm for the reference case (only aluminum material) as seen at the top of *Figure 2*. The thickness of the material was selected after a preliminary study in which all relevant parameters (i.e. engine speed, material properties…) were considered. The penetration of the temperature oscillation in the solid was calculated following the method used by Andruskiewicz et al. [29]. The positions at which oscillation is attenuated up to 10% ($depth_{10\%}$) and 1% ($depth_{1\%}$) of the surface temperature oscillation were calculated using both operating conditions described below as a boundary conditions. From these calculations, it can be noticed that the temperature oscillation vanishes very quickly and penetrates barely 1 mm in the solid. For instance, considering the most critical operating condition (1500 rpm and 14 bar of BMEP), the $depth_{10\%}$ is around 0.18 mm and the $depth_{1\%}$ is close to 0.36 mm. Thus, although 1 mm is clearly smaller than the actual material thicknesses between the combustion chamber and the surfaces in contact with the oil/coolant, instantaneous results will not be affected by this hypothesis, as indeed the model meets the physical restrictions for both operating conditions used in this research work.
- 1 mm of aluminum material plus the thickness of the coating for the case of the coated surface, as seen at the bottom of *Figure 2*.

In both cases, the boundary conditions (also represented in *Figure 2*) used were:

- On the left-hand side of the bar, the instantaneous gas temperature and the heat transfer coefficient obtained from an in-house combustion diagnosis tool [30][31] were fixed. This tool calculates both instantaneous variables from the in-cylinder pressure by means of the energy conservation equation and some simplifications. The energy equation was solved assuming uniform pressure and temperature throughout the whole combustion chamber volume. Both thermodynamic values were obtained for a CI diesel engine running at 1500 rpm and 8-14 bar of BMEP. As a reference, *Table 1* contains the most relevant engine specifications and *Table 2* show the main characteristics of the injector.
- On the right-hand side of the bar a constant temperature of 90°C was fixed, representing the nominal coolant temperature of the engine.

Figure 2: *Scheme of the simple bar with the boundary conditions.*

Table 1: *Engine specifications.*

Engine Type	4 stroke, 4 valves, direct injection
Number of cylinders [-]	1
Displaced volume [cm^3]	477
Stroke [mm]	90.4
Bore [mm]	82
Piston bowl geometry [-]	Re-entrant
Compression ratio [-]	17.1:1
Rated power [kW]	27.5 @ 4000 rpm
Rated torque [Nm]	80 @ 2000-2750 rpm

Table 2: *Characteristics of the direct fuel injector*

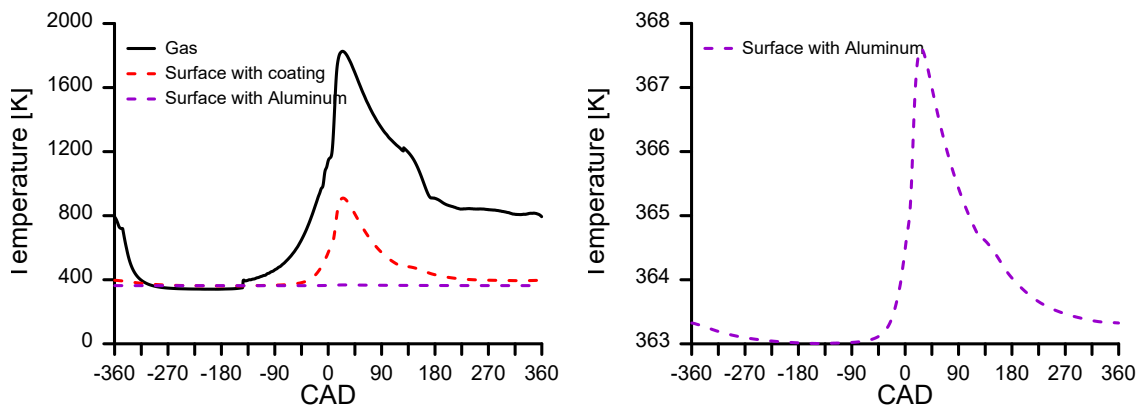| Direct injector	
Actuation Type [-]	Solenoid
Steady flow rate @ 100 bar [cm^3/min]	880
Included spray angle [°]	148
Number of holes [-]	7
Hole diameter [μm]	141
Maximum injection pressure [bar]	1600

As a first example, an ideal coating with 100 μm thickness was considered for the calculation. The coating properties are presented in *Table 3*, together with those of the aluminum. This simple calculation will give an idea of the maximum gain that might be expected with a coated surface.
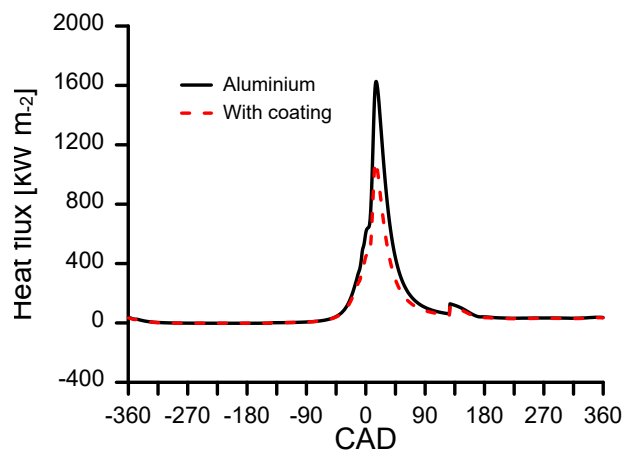
Table 3: *Solid properties.*

Material	Density, ρ [kg m-3]	Specific heat, C_p [J kg-1 K-1]	Conductivity, k [W m-1 K-1]
Aluminum	2659	871	144
Ideal coating	1000	100	0.1

Figure 3 shows the temperatures calculated by the model for conditions representative of the diesel engine running at 1500 rpm and 8 bar BMEP. In the plot on the left, the in-cylinder gas temperature that has been used as a boundary condition (black line), and the surface temperatures calculated by the model considering both a coated surface (red dashed line) and the baseline case aluminum surface without coating (purple dashed line) are shown.

The results show that for the coated surface, the response is a temperature swing of about 1/3 of the gas temperature with some delay, which should be governed by an equivalent Biot number, as in the simplified theoretical model (Eq. 7). For the baseline configuration, the aluminum surface temperature remains practically constant, with a negligible peak temperature variation of about 5ºC, as seen in the right plot of *Figure 3*, where a zoom of the aluminum surface temperature variation is plotted. This figure further validates the numerical model since many authors reached similar results (in terms of maximum wall temperature swing) when estimating the wall temperature of similar engines operating at comparable operation conditions [20][21][22][23].

Figure 3: *Instantaneous temperatures predicted by the model at 1500 rpm and 8 bar BMEP: comparison between uncoated (Aluminum) and coated engine (left) and zoom of wall temperature swing of uncoated engine (right).*

Figure 4: *Instantaneous heat flux predicted by the model at 1500 rpm and 8 bar BMEP: comparison between uncoated (Aluminum) and coated engine.*

Figure 4 shows a comparison between the instantaneous heat fluxes calculated for the uncoated (black line) and coated (red dashed line) bars described previously. The ratio between the heat flux with the coated and aluminum surfaces is 0.73 for the operating condition at 1500 rpm and 8 bar BMEP. This means that in this case a heat gain of 27% may be expected.

2.2. Validation of the 1D HTM model

The numerical model was validated by comparison with the analytical solution of the simple case defined in *Figure 5*. In this theoretical problem [28], the following hypotheses are assumed:

- The calculation domain is a semi-infinite solid, so that the heat transfer is one-dimensional.

- The solid consists of one material with constant conductivity (k), density (ρ) and specific heat (C_p).

- The gas temperature (T_g) on the left-hand side of the solid varies as defined by Eq 1.

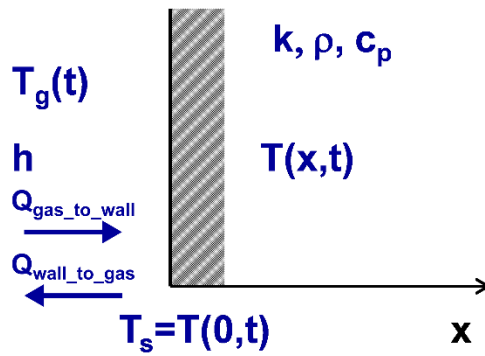- The heat transfer coefficient between the gas and the solid surface is constant.

Figure 5: *Problem scheme for the model validation.*

Then,

$$T_g(t) = T_{gm} + \Delta T_g \cos(\omega t) \qquad\qquad \text{Eq. 1}$$

Where *t* is time, T_{gm} is the average gas temperature, ΔT_g is the amplitude of gas temperature and ω is the gas temperature period:

$$\omega = 2\pi n f_0 \qquad\qquad \text{Eq. 2}$$

Where *n* represents the harmonic number and f_0 is the fundamental frequency.

Taking into account the hypotheses mentioned above, the boundary condition on the left-hand side of the solid surface is:

$$\dot{q} = \text{h}\left(T_g - T_s\right) = -\text{k}\frac{\partial T}{\partial x}\bigg|_{x=0} \qquad\qquad \text{Eq. 3}$$

Where T_s represents the solid temperature at the surface and T represents the solid temperature at any point of the solid. In this case, the unsteady one-dimensional heat conduction equation is solved in the semi-infinite solid

$$\frac{\partial T(x,t)}{\partial t} = \alpha \frac{\partial^2 T(x,t)}{\partial x^2}$$

Eq. 4

Where α represents the thermal diffusivity:
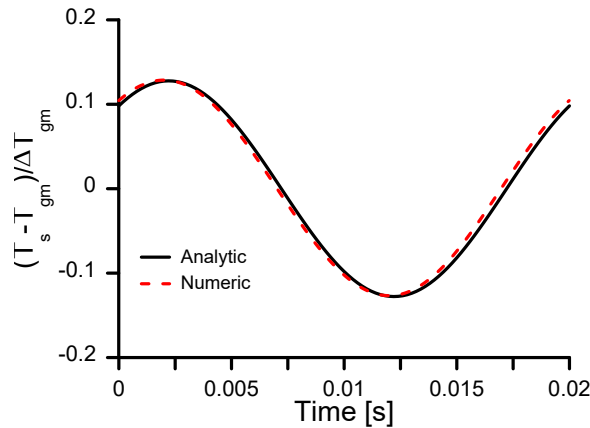
$$\alpha = \frac{k}{\rho c_p}$$

Eq. 5

So, the analytical solution for the instantaneous temperature at the solid surface [28] is:

$$\frac{T(0,t)-T_{gm}}{\Delta T_g} = \frac{Bi}{(Bi^2+2Bi+2)^{1/2}} \cdot \cos\left(\omega t - \tan^{-1}\frac{1}{1+Bi}\right)$$

Eq. 6

Where both the amplitude of the surface temperature and the phase shift depend only on the Biot number, which can be written as

$$Bi = \frac{h}{k}\sqrt{\frac{\alpha}{\pi n f_0}} = \frac{h}{\sqrt{k\rho c_p \pi n f_0}}$$

Eq. 7

The results obtained by using both approaches considering the same boundary conditions are compared in *Figure 6*. The good agreement between both temperatures confirms the reliability of the numerical model for predicting the evolution of the surface temperature.

Figure 6: *Surface temperature of the numerical model compared with the analytic solution with same BC.*

2.3. Virtual engine model

The 1D HTM is also integrated in the engine thermal model described in [32]. This model which couples the thermodynamic model described in [33][34] with the predictive combustion model proposed by Arrègle et al. [35], was used to estimate the engine outputs as the configuration of the coated surfaces (cylinder head, piston…) were modified.

This complex model has several sub-models with a series of constants that need to be adjusted. In addition to fit the values of the Wiebe constants in the combustion model, it is

necessary to set the values of the heat transfer model and the deformation model constants. The adjustment was done using experimental measurements obtained through a broad parametric study of the engine, both in motoring and combustion operating conditions. This fitting procedure is described in [32] and [35] for the thermodynamic and combustion models, respectively.

The validation of this virtual engine model was previously published in [36] and comprises a wide range of operating conditions. Results showed a good overall performance between the modeled and experimental results (considering both stationary and transient conditions), when the most relevant engine outputs such as intake pressure, turbine inlet/outlet temperatures, coolant temperature, oil temperatures and torque are changed.

2.4. Heat fluxes definition

In the following sections different heat fluxes will be analyzed. The meaning of each of these heat fluxes is the following:

- As shown in *Figure 5*, the heat flow from the gas to the walls (i.e. when the temperature of the gas is higher than the wall temperature) is referred as $Q_{gas\_to\_wall}$.
- Similarly, the heat flux from wall to gas is denoted as $Q_{wall\_to\_gas}$. This heat transfer occurs when the temperature of the gas is lower than the wall temperature. For instance, when the combustion chamber surfaces with a high thermal load (during the operation at high loads) contribute to the in-cylinder flow temperature increase.
- Total heat loss is the heat transferred between the in-cylinder gas and the walls (considering both $Q_{gas\_to\_wall}$ and $Q_{wall\_to\_gas}$) during a thermodynamic cycle.

$$Q_T = Q_{gas\_to\_wall} - Q_{wall\_to\_gas} \qquad \text{Eq. 9}$$

- The performance of the coating material is evaluated by the "heat insulation rate" or "heat gain" (both denominations will be used from now on), which is defined in Eq. 10. This parameter represents the gain in terms of the total heat transfer obtained with a coated surface (Q_T^{coat}) with respect to the baseline wall material of aluminum (Q_T^{alu}).

$$\text{Heat gain} = 1 - \frac{Q_T^{coat}}{Q_T^{alu}} \qquad \text{Eq. 10}$$

- The effect of the coating material on the heat transferred from the walls to the gas ($Q_{wall\_to\_gas}$) can be quantified by the "negative ratio" parameter (Eq. 11), which relates the heat transferred to the gas with a coated surface ($Q_{wall\_to\_gas}^{coat}$) with respect to the baseline aluminum ($Q_{wall\_to\_gas}^{alu}$) configuration:

$$\text{Negative ratio} = \frac{Q_{wall\_to\_gas}^{coat}}{Q_{wall\_to\_gas}^{alu}} \qquad \text{Eq. 11}$$

According to this expression, the negative ratio is larger than 1 when the $Q_{wall\_to\_gas}$ using a given coating is larger than that obtained with the aluminum configuration. Thus, a negative ratio of 1.1 means that the $Q_{wall\_to\_gas}$ is 10% larger than the baseline aluminum configuration.
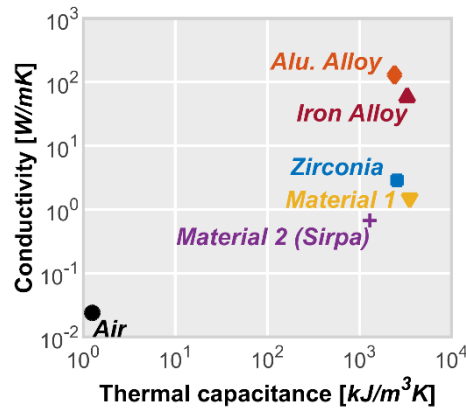
2.5. Methodology

After the implementation and validation of the model, advantage was taken from its outputs to better understand the trade-off between the heat insulation rate and the negative ratio for different coating materials and thicknesses.

First, the 1D HTM was used to calculate both the $Q_{gas\_to\_wall}$ and $Q_{wall\_to\_gas}$ heat flows for different coating properties. The analysis of the results particularly focuses on the total insulation rate, the heat insulation gain and the negative ratio. The coating characteristics have been varied with respect to baseline values chosen from preliminary studies and data available in the literature [13][17][18][19]. The current methodology can be summarized as follows:

- The study was performed for two different operating conditions: 1500 rpm - 8 bar BMEP (medium load) and 1500 rpm - 14 bar BMEP (high load). Instantaneous heat transfer coefficient (h_{gas}) and instantaneous gas temperature (T_{gas}) were estimated from the in-house combustion diagnosis tool [30][31] for the diesel engine considered. These data remained the same for all simulations. Hence, the possible effect of the coating on in-cylinder thermodynamics has not been taken into account.
- The conductivity range of variation was between 0.5 and 2 $Wm^{-1}K^{-1}$ with a step of 0.06 $Wm^{-1}K^{-1}$, i.e. 26 different values of conductivity.
- The coating thickness was varied between 80 and 300 μm with a step of 8.8 μm, i.e. 26 different values of coating thickness.
- Two values were given to the thermal capacitance ($\rho\, c_p$): 1300 (Material 1 thermal capacitance) and 3500 (Material 2 thermal capacitance) kJ m^{-3} K^{-1}. From preliminary studies, it was determined that the effect of the conductivity and the coating thickness on heat flux is notably higher than that of the thermal capacitance. Thus, in order to avoid excessive computational time, only these two values were considered. The properties of the different materials (coatings and baseline) used in the simulation are presented in *Table 4*. Additionally, in *Figure 7*, the selected coatings are compared with other relevant materials.
- In order to reproduce real engine conditions, different boundary conditions were applied on the cylinder head and the piston surface. While the same cyclic transient heat flux was imposed at each the surface in contact with the gas, the constant thermal sinks considered for the backside of the material were different: the measured oil temperature was used as boundary condition for the piston, whereas the coolant temperature was used for the cylinder head.

Table 4: *Thermo-physical properties of the different materials used in the simulation (source for Material 2 [18]).*

Material	Thermal capacitance, ρC_p [kJ m^{-3} K^{-1}]	Conductivity, k [W m^{-1} K^{-1}]
Material 1	3500	1.5
Material 2	1300	0.67

Figure 7: *Comparison of different material properties [18].*

In summary, a total of 2028 cases have been calculated, with different coating characteristics for each of the two operating conditions considered.

After this initial study, that helped to determine realistic ranges of k and material thicknesses, further analysis was made to predict the thermal flows across the cylinder parts covered with the insulation and, specially, to determine the effect of the coating on engine indicated efficiency. The 1D HTM coupled with the virtual engine model was used for this purpose.

Calculations have been performed for the standard engine configuration (aluminum) and for the coated surfaces configuration. The impact of the coating may thus be quantified not only in terms of indicated efficiency, but also in terms of volumetric efficiency and/or other relevant engine outputs.

The global methodology of this second approach has some similarities with the previous methodology:

- Two different operating conditions representative of medium (1500 rpm-8 bar BMEP) and high load (1500 rpm-14 bar BMEP).
- Two different coatings: materials defined in *Table 4* were used for comparison.
- The coating thickness range between 100 and 300 μm was considered with a step of 100 μm, i.e. 3 different values of coating thickness.
- Only the surface of the piston, cylinder head and the bottom part of the valves are totally coated. Despite the application of this technology in the bottom part of the valves has some inherent issues related to the different material properties, mechanical stresses, the idea here is to establish the maximum level of gain with the largest amount of coated surface. The liner made of steel remains as in the standard configuration since the possible coating surface would be destroyed after several engine cycles due to the piston rings friction.
- The injection settings used in the model were those of the standard configuration.
- The boundary conditions at oil/coolant sides (defined by constant thermal sinks) are placed at a "realistic" location. The thickness of the aluminium was fixed depending on the node position and its length (the real distance between the combustion chamber and the oil/coolant galleries).

In this case, only a set of 12 simulations was performed to minimize the computational cost.
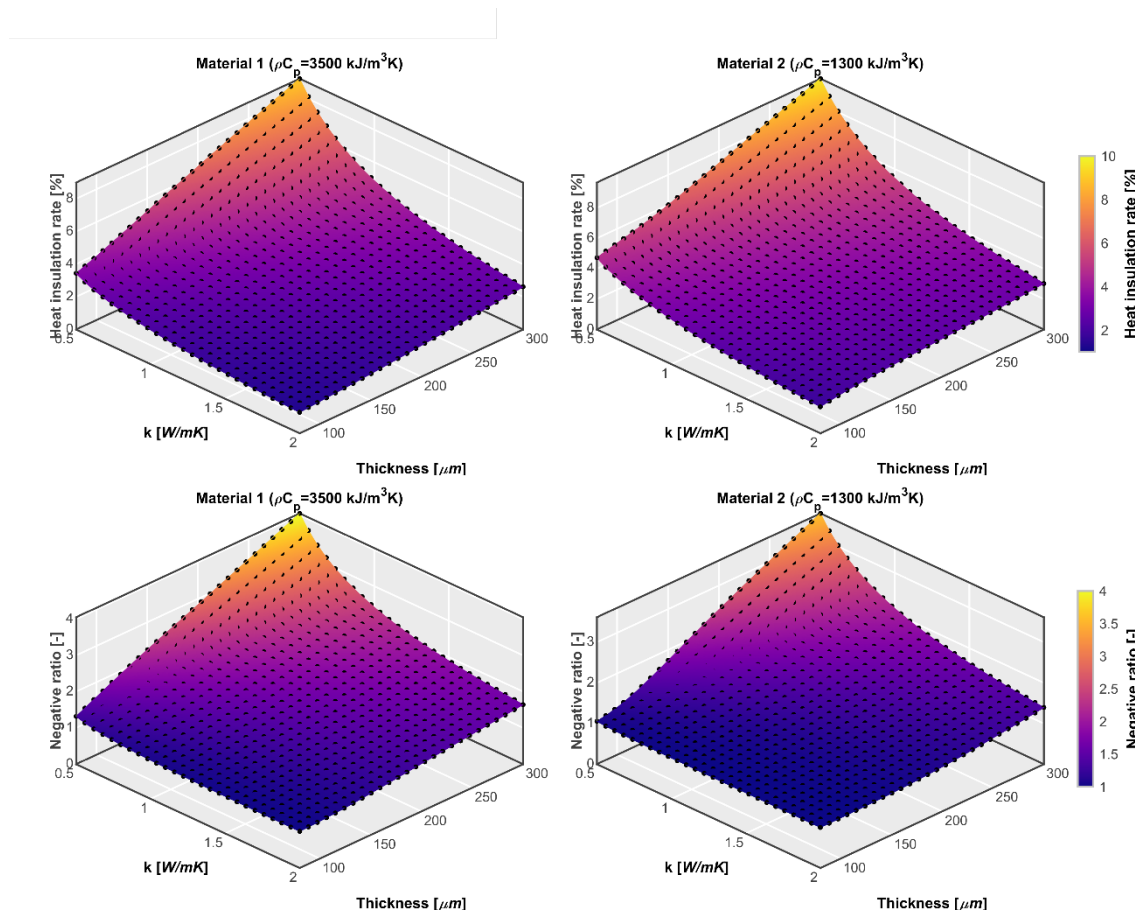
3. Results and discussion

In this section, the results obtained from the studies described in Section 2.5 are presented and discussed. First, the impact of the coating properties on the engine heat transfer fluxes is analyzed in detail. Then, the subsequent effect on the engine outputs is studied and discussed. Finally, the possible gains in both heat insulation and thermal efficiency are quantified and further discussion about the potential benefits of applying these heat barriers are further discussed.

3.1. Impact of coating properties on the engine heat transfer

For the operating conditions considered, the heat losses were calculated for each of the 2028 coating configurations, as well as the total and heat insulation gain and negative ratio.

For each of the two thermal capacitances considered a piecewise cubic interpolation of the data was applied to generate surface plots of both the heat insulation gain and negative ratio in function of the coating conductivity and thickness. As an example of these plots, *Figure 8* shows the heat insulation rate and the negative ratio obtained with the two thermal capacitance levels at 1500 rpm and 8 bar BMEP.
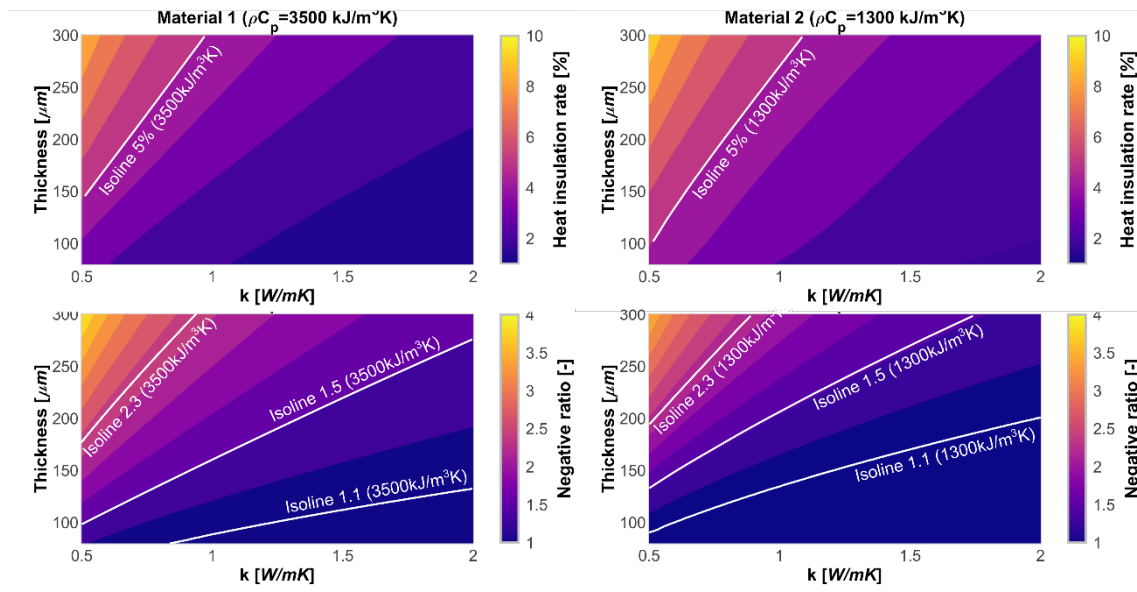

Figure 8: *Maps of the heat insulation rate (top) and negative ratio (bottom) obtained with the 1D HTM for the two ρC_p selected at 1500 rpm and 8 bar BMEP.*

The maps of *Figure 9* were then obtained from the surface plots of *Figure 8*. The white lines in these plots indicate the set of thicknesses and conductivities for which a heat gain of 5% or 1.1 of negative ratio (1.3 and 1.5 isolines are drawn as well for further studies) can be obtained

with a capacitance of 1300 and 3500 kJ m-3 K-1. These white lines will be used in the following graphs in order to identify the most favorable regions on the map.

Similar surface plots and maps were obtained for each capacitance value (3500 and 1300 kJ/m^{3}K) and operating condition (1500@8 and 1500@14) by means of the same procedure. With this information graphs showing the trade-off between the heat insulation rate and the negative ratio were drawn. *Figure 10* shows the trade-off graphs corresponding to the total heat insulation rate for the two operating conditions. The blue bands in these plots indicate the characteristics of the coating required to achieve 5% of total heat insulation rate, while the grey bands represent the corresponding negative ratio.
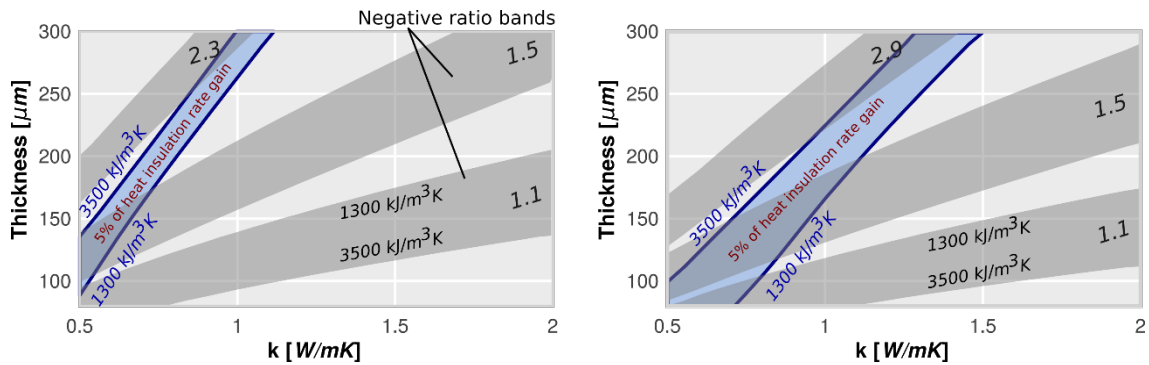

Figure 9: *Determination of the heat insulation iso-rate lines (top) and negative ratio (bottom) obtained with the 1D HTM for the two selected materials at 1500 rpm and 8 bar BMEP.*

It may be inferred from these plots that the thickness of a coating material with k=1.5 W m^{-1} K^{-1} and ρC_p=3500 kJ m^{-3} K^{-1} (which corresponds to the limit defined by Material 1) must be larger than 300 μm to be in the 5% total heat insulation rate gain. In these conditions, the negative ratio is much higher than 2 and this could have very significant effects on the volumetric efficiency, since the Q$_{wall-to-gas}$ value doubles the reference aluminum configuration. At this point, the effect of the wall-to-gas heat flux has not yet been evaluated and therefore this arbitrary value should not be considered as a limit beyond which the volumetric efficiency loss is significant. Moreover, these plots show that low values of both conductivity and capacitance are compulsory if a 10% increase of the Q$_{wall\_to\_gas}$ is allowed (1.1 of negative ratio).
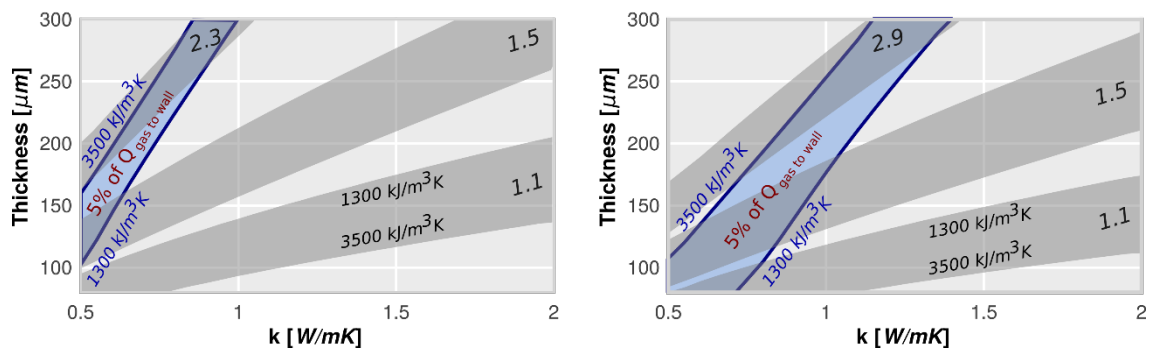
Regarding the differences between operating conditions, specifically when the engine load is changed, it seems that the requirements on the material properties are slightly lower as the engine load increases. Note that the blue band is wider in the right graph where the engine load is 14 bar BMEP. In addition to this, the wider blue band allows reaching regions in which 5% of heat insulation gain and a 1.1 of negative ratio is guaranteed. These conditions, characterized by low values of both material thickness and conductivity, are unattainable at lower loads. Therefore, a suitable combination of both parameters offers the same level of heat insulation gain, but with lower negative impact on the volumetric efficiency at higher loads. However, at these conditions, the penalty in negative ratio is higher as the material

thickness is increased. Indeed, materials with the largest thickness that achieve 5% of heat insulation gain hardly reach 2.3 of negative ratio at low load, whereas they easily exceed 2.9 at high loads. Thus, it is critical to keep the material thickness at small values, ensuring that volumetric efficiency is not excessively compromised throughout the whole operating range.

The trade-off graphs for the heat insulation rate are shown in *Figure 11*. In these plots, the blue bands (which are slightly wider than in the previous graphs) correspond to the coating characteristics required to achieve 5% of heat insulation rate ($Q_{gas\_to\_wall}$). Regarding the coating material referred in the paragraph above, the same remarks are also valid for the heat gain, emphasizing then the greater relevance of the $Q_{gas\_to\_wall}$ versus $Q_{wall\_to\_gas}$ flows.

Figure 10: *Trade-off between heat insulation rate and negative ratio. Left hand side: 1500 rpm and 8 bar BMEP, right hand side: 1500 rpm and 14 bar BMEP.*

Figure 11: *Trade-off between heat insulation rate and negative ratio. Left hand side: 1500 rpm and 8 bar BMEP, right hand side: 1500 rpm and 14 bar BMEP.*
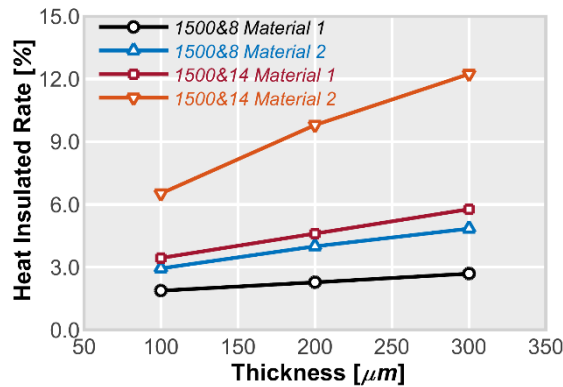
3.2. Effects on the engine performance

After understanding how the coating properties affect the total heat fluxes, examining how they condition the engine performance is the next natural step in the investigation. The results of the impact of the coating on the mentioned efficiencies will be shown in two different ways:

- On one hand, as the difference between the efficiency obtained with coating and the efficiency obtained with the standard configuration (aluminum).
- On the other hand, as the ratio between the efficiency obtained with coating and the efficiency obtained with the standard configuration.

Prior to analyzing the engine performance, the effect of the coating thickness on heat insulation is shown in *Figure 12*. In this figure, the heat rate is plotted against different materials, thicknesses and operating conditions. Although these trends have already been discussed in the previous section (*Figure 10* and *Figure 11*), they are interesting from the point

of view of the complete model (coupling both thermodynamic and thermal modelling) validation. Specifically, if we look at the values of the heat insulation rate for Material 1, only the highest load condition and material thickness exceeds 5%. However, Material 2 offers higher levels of insulation rate in both operating conditions, exceeding the threshold of 5% at high load conditions with any material thickness considered. This is consistent with the results presented in the previous section, therefore validating the results of the model.
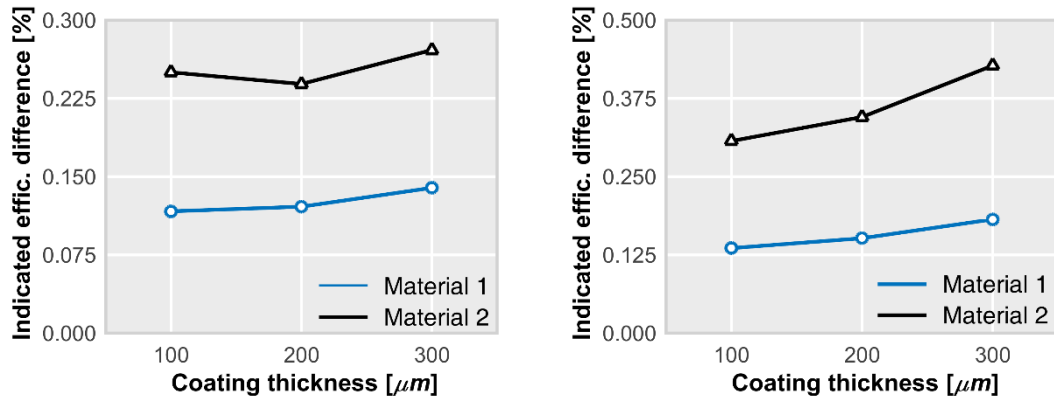

Figure 12: *Heat insulated rate gains for the two selected materials, operating conditions and different material thicknesses.*

Figure 13 shows the absolute differences obtained with respect to the standard configuration in indicated efficiency for the two operating points. In both cases the trends are quite similar. As expected, the gain using Material 2 is higher than that obtained with the Material 1 coating. The gain does not vary linearly with coating thickness: indeed, the gain in indicated efficiency obtained with a coating of 100 μm thickness (with respect to 0 thickness = aluminum) is clearly more significant than the additional gain that may incur for larger values of the thickness.
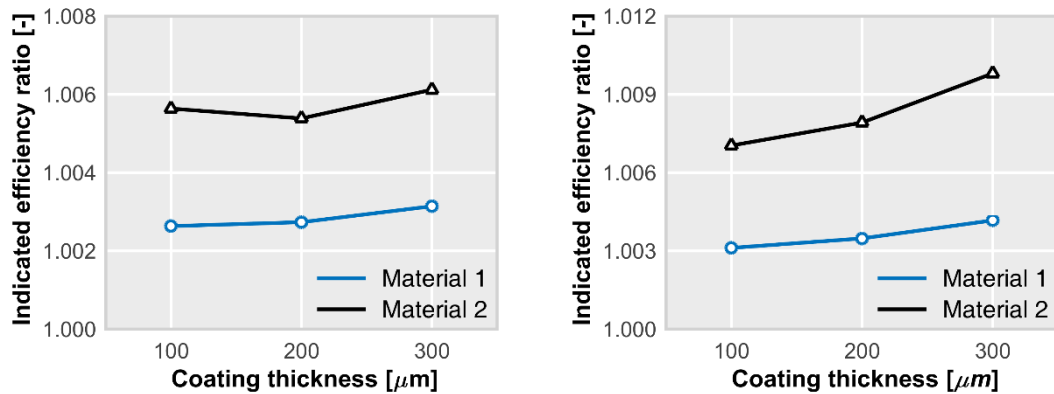
Even so, results show that for a 100 μm thickness a gain of ≈ 0.25-0.3% on indicated efficiency may be expected when using Material 2 coating, but this gain falls to ≈ 0.11-0.13 % if Material 1 is used. The observed change in indicated efficiency is mostly due to the heat insulated rate obtained with the coating. The $Q_{wall\_to\_gas}$ flow caused by wall insulation, does not affect indicated efficiency significantly, since its effect on volumetric efficiency is not relevant, as will be shown in further analyses presented below (see *Figure 16*, *Figure 17* and *Figure 18*).

The ratio of indicated efficiency obtained with coated surfaces versus the indicated efficiency obtained in the standard configuration is shown in *Figure 14*. For 100 μm thickness an increase in this ratio by about 0.6% to 0.7% is observed with the Material 2 coating. However, an increase of only 0.2% to 0.3% is obtained when using Material 1, depending on the operating point. The main reasons of this increment are the same as mentioned for *Figure 13*.
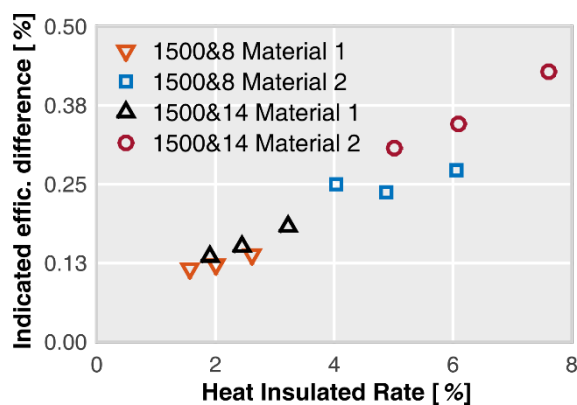
Figure 15 shows the evolution of the indicated efficiency difference as the heat insulation rate increases with the different coating materials and thicknesses considered in this analysis. These results show that the indicated efficiency increases almost proportionally with the insulation rate rise. Finally, the results show that the higher increase of the indicated efficiency is obtained with Material 2 at both operating conditions. This fact is due to the higher insulation rate achieved with this material due to its lower conductivity and capacity. All these trends are in line with the works referred to in the introduction performed by Heywood [20], Rakopoulos et al. [21], Chang et al. [22] and Kikusato et al. [23]. In all of them, the potential gains obtained by using coating materials are marginal and disagree with the results published by Toyota [13][17][18][19].

Figure 13: *Indicated efficiency difference between coated engine walls and standard configuration. Left hand side: 1500 rpm and 8 bar BMEP, right hand side: 1500 rpm and 14 bar BMEP.*

Figure 14: *Indicated efficiency ratio between coated engine walls and standard configuration. Left hand side: 1500 rpm and 8 bar BMEP, right hand side: 1500 rpm and 14 bar BMEP.*

Figure 15: *Indicated efficiency difference between coated engine walls and standard configuration vs Heat insulation rate, for both operating conditions: 1500 rpm & 8 bar BMEP and 1500 rpm & 14 bar BMEP. The three symbols for each combination of material/load are different coating thicknesses.*

The effect of the coating on volumetric efficiency is shown in *Figure 16* and *Figure 17* for the two operating points. The former shows the differences obtained with respect to the standard

configuration for both engine operating points. It may be observed that the volumetric efficiency decreases with increasing coating thickness. This effect is due to the increase in $Q_{wall\_to\_gas}$ flux during the intake stroke, which leads to a decrease of the in-cylinder air density and, therefore, the model predicts a lower intake of mass flow. As expected, the effect of using Material 1 is higher than that obtained with the Material 2. For the case of 100 µm thickness the observed reductions are 0.31 to 0.53 % for Material 1 and 0.08 to 0.20 % for the Material 2, depending on the considered operating point.

As observed in *Figure 17*, the volumetric efficiency ratio for the case of 100 µm shows a reduction of about 0.3 to 0.5 % for the Material 2 coating, while this reduction is only of 0.05 to 0.2% for the Material 1 coating, depending on the operating point.

Figure 16: *Volumetric efficiency difference between coated engine walls and standard configuration. Left hand side: 1500 rpm and 8 bar BMEP, right hand side: 1500 rpm and 14 bar BMEP.*
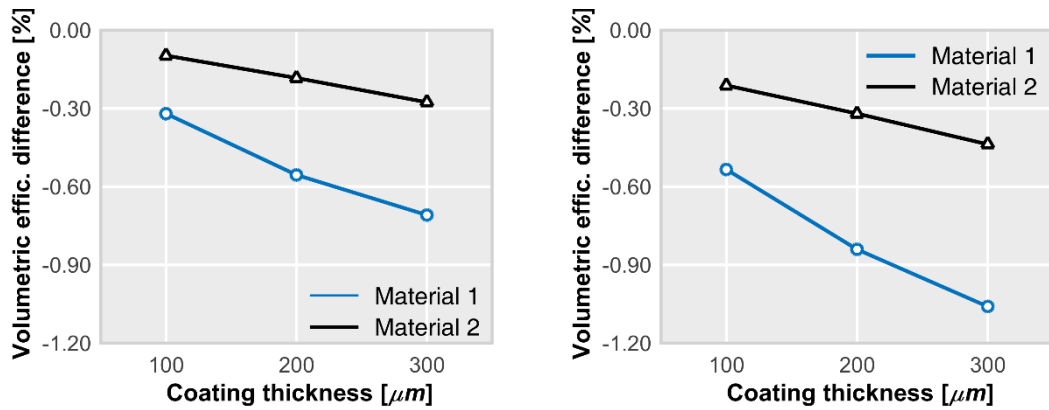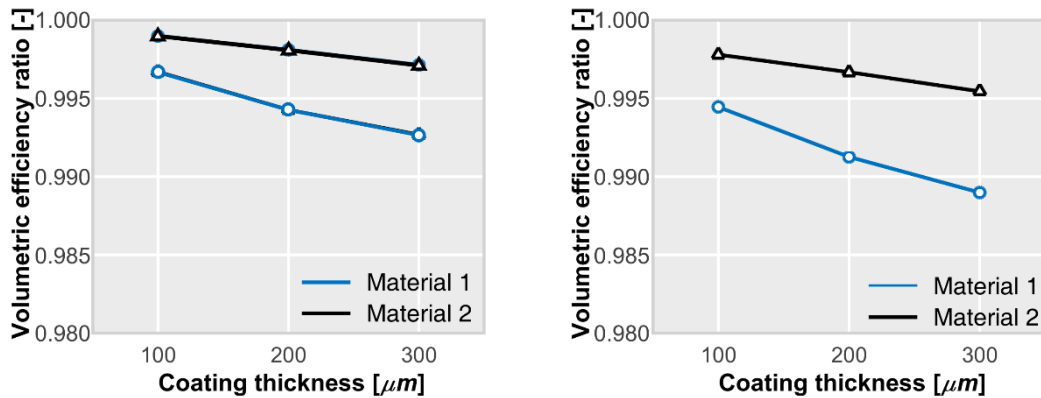

Figure 17: *Volumetric efficiency ratio between coated engine walls and standard configuration. Left hand side: 1500 rpm and 8 bar BMEP, right hand side: 1500 rpm and 14 bar BMEP.*

Finally, *Figure 18* shows the variation of the volumetric efficiency difference with the negative ratio for the different coating materials and thicknesses considered in this study. The results show that the volumetric efficiency reduces in proportion to the increase of the negative ratio. In addition, the reduction rate is higher at lower load and there is a higher impact on volumetric efficiency with Material 2, due to its low conductivity and capacitance. As it can be

seen in this figure, there is range for the negative ratio parameter in which the volumetric efficiency is not worse than the reference case (aluminum configuration). By extrapolating the data of the materials used it is possible to determine that this limit is around 1.1, therefore keeping the negative ratio below 1.1 the volumetric efficiency of the engine does not deteriorate.

Figure 18: *Volumetric efficiency difference between coated engine walls and standard configuration vs negative ratio, for both operating conditions: 1500 rpm & 8 bar BMEP and 1500 rpm & 14 bar BMEP. The three symbols for each combination of material/load are different coating thicknesses.*

4. Conclusions

An approach to estimate the heat transfer losses of internal combustion engines equipped with advanced coating materials has been presented in this paper. A 1D numerical model for predicting the heat transfer through coated surfaces has been developed and coupled with a complete thermodynamic engine model to predict the effect of coating the piston and cylinder head of an engine on both heat fluxes and engine performance. The 1D model has been validated against analytical results of a simplified problem and qualitatively compared with several works performed by other authors. The model has been set up using data from a compression-ignition diesel engine representative of the current trends in the light-duty automotive sector. For this purpose, two operating conditions were specifically chosen. Hence, the conclusions obtained and summarized below are not necessarily to the whole engine operation map.

In addition, calculations were performed assuming that the cylinder charge temperature is homogenous, and the heat transfer coefficient is uniform along the gas exposed surfaces. This has some implications as these hypotheses are not strictly fulfilled in real engine conditions, especially in CI diesel engines due to the "static" nature of combustion (combustion takes place mainly in stabilized sprays). Although in this research the effect of spatiality has not been studied due to these limitations, it could be evaluated by combining the 1D HTM with more advanced methods that will supply the correct BCs for different positions within the combustion chamber (i.e. 3D Computational Fluid Dynamic simulations).

The studies performed using the 1D numerical model have shown:

- The coating thickness affects both the gas-to-wall and wall-to-gas heat flows. In order to avoid excessive $Q_{wall\_to\_gas}$ (1.1 of negative ratio), the thickness must be kept small. The results indicate that a limit of approximately 100 μm must be considered.

- With this thickness of 100 μm the Material 2 properties allow an insulation heat rate of approximately 5%, but this rate is reduced to 2% with the Material 1 coating for the two considered operating points.

- Trade-off graphs show that for achieving 5% of heat insulation rate with a given coating conductivity, higher values of capacitance will induce higher wall-to-gas heat flux.

- For heat insulation levels of 5%, the lowest negative ratio may only be achieved by reducing the three parameters conductivity, capacitance and thickness.

- The range of conductivity-capacitance combinations for achieving 5% of heat insulation ratio while keeping the negative ratio at 1.1 (to keep the volumetric efficiency at the same level as the aluminium engine configuration) is limited to materials with capacitances similar to that of named Material 2 coating. Higher conductivity-capacitance range like that of the Material 1 would lead to inadmissible negative ratio, since it would be necessary to increase the thickness significantly.

The combination of the 1D HTM with a complete thermodynamic/thermal model also allowed drawing the following conclusions:

- In the case of indicated efficiencies: a maximum of 0.3% of fuel input energy may be recovered with 100 μm of Material 2 coating on the piston and cylinder-head; only 0.13% with the Material 1 under the same conditions.

- A reduction in volumetric efficiency has been predicted with both coatings. Results shown that this reduction is not critical (< 1% with respect to the aluminium case), even considering the worst combination of material/load/thickness (< 1% respect to the aluminium case), because the wall-to-gas heating period is too short in comparison with the intake phase. Moreover, there is a range for the negative ratio parameter (from 1 to 1.1) in which the volumetric efficiency is not worse than the reference case (aluminium case).

References

[1] A. Roy, C. Mishra, S. Jain, N. Solanki. A New Design to Achieve Variable Compression Ratio in a Spark Ignition Engine. Chandrasekhar U., Yang LJ., Gowthaman S. (eds) Innovative Design, Analysis and Development Practices in Aerospace and Automotive Engineering (I-DAD 2018).

[2] H. Ryo, Y. Hiromichi, HCCI combustion in a DI Diesel engine, in: SAE Technical Paper, vol. 2003-01-0745.

[3] J. Benajes, R. Novella, D. De Lima, P. Tribotte, Investigation on multiple injection strategies for gasoline PPC operation in a newly designed 2-stroke HSDI compression ignition engine, SAE Int. J. Eng. 8 (2015) 758–774.

[4] A.J. Torregrosa, A. Broatch, R. Novella, J. Gomez-Soriano, & L.F. Mónico. (2017). Impact of gasoline and Diesel blends on combustion noise and pollutant emissions in Premixed Charge Compression Ignition engines. Energy, 137, 58-68.

[5] N. F. O. Al-Muhsen, Y. Huang, G. Hong. Effects of direct injection timing associated with spark timing on a small spark ignition engine equipped with ethanol dual-injection. Fuel 239 (2019): 852-861.

[6] A. Broatch, P. Olmeda, X. Margot, and J. Gomez-Soriano. Numerical simulations for evaluating the impact of advanced insulation coatings on H2 additivated gasoline lean combustion in a turbocharged spark-ignited engine. Applied Thermal Engineering 148 (2019): 674-683.

[7] M. Wu, Y. Pei, J. Qin, X. Li, J. Zhou, Z.S. Zhan, Q.-y. Guo, B. Liu, T.G. Hu, Study on methods of coupling numerical simulation of conjugate heat transfer and in-cylinder combustion process in GDI engine, SAE Technical Paper, 2017-01-0576.

[8] F. Berni, G. Cicalese, S. Fontanesi, A modified thermal wall function for the estimation of gas-to-wall heat fluxes in CFD in-cylinder simulations of high performance spark-ignition engines, Applied Thermal Engineering 115 (2017) 1045–1062.

[9] L. Zhang, Parallel simulation of engine in-cylinder processes with conjugate heat transfer modeling, Applied Thermal Engineering. 142 (2018) 232–240.

[10] Poubeau, A., Vauvy, A., Duffour, F., Zaccardi, J.-M., Paola, G. de, & Abramczuk, M. (2019). Modeling investigation of thermal insulation approaches for low heat rejection Diesel engines using a conjugate heat transfer model. International Journal of Engine Research, 20(1), 92–104. https://doi.org/10.1177/1468087418818264

[11] P. Kundu, R. Scarcelli, S. Som, A. Ickes, Y. Wang, J. Kiedaisch, M. Rajkumar, Modeling heat loss through pistons and effect of thermal boundary coatings in diesel engine simulations using a conjugate heat transfer model, SAE Technical Paper, 2016-01-2235.

[12] C.D. Rakopoulos, D.C. Rakopoulos, G.C. Mavropoulos, E.G. Giakoumis, Experimental and theoretical study of the short term response temperature transients in the cylinder walls of a diesel engine at various operating conditions, Applied Thermal Engineering. 24 (5) (2004) 679–702.

[13] K. Fukui, Y. Wakisaka, K. Nishikawa, Y. Hattori, H. Kosaka, A. Kawaguchi, Development of instantaneous temperature measurement technique for combustion chamber surface and verification of temperature swing concept, SAE Technical Paper, 2016-01-0675.

[14] Kawaguchi, A., Wakisaka, Y., Nishikawa, N., Kosaka, H., Yamashita, H., Yamashita, C., … Tomoda, T. (2019). Thermo-swing insulation to reduce heat loss from the combustion chamber wall of a diesel engine. International Journal of Engine Research, 20(7), 805–816. https://doi.org/10.1177/1468087419852013.

[15] Powell, T., O'Donnell, R., Hoffman, M., Filipi, Z., Jordan, E. H., Kumar, R., & Killingsworth, N. J. (2019). Experimental investigation of the relationship between thermal barrier coating structured porosity and homogeneous charge compression ignition engine combustion. International Journal of Engine Research. https://doi.org/10.1177/1468087419843752.

[16] Somhorst, J., Oevermann, M., Bovo, M., & Denbratt, I. (2019). Evaluation of thermal barrier coatings and surface roughness in a single-cylinder light-duty diesel engine. International Journal of Engine Research. https://doi.org/10.1177/1468087419875837.

[17] H. Kosaka, Y. Wakisaka, Y. Nomura, Y. Hotta, M. Koike, K. Nakakita, A. Kawaguchi, Concept of "temperature swing heat insulation" in combustion chamber walls, and appropriate thermo-physical properties for heat insulation coat, SAE Int. J. Engines 6 (1) (2013) 142–149.

[18] Y. Wakisaka, M. Inayoshi, K. Fukui, H. Kosaka, Y. Hotta, A. Kawaguchi, N. Takada, Reduction of heat loss and improvement of thermal efficiency by application of temperature swing insulation to direct-injection diesel engines, SAE Int. J. Engines 9 (3) (2016) 1449–1459.

[19] T. Kogo, Y. Hamamura, K. Nakatani, T. Toda, et al., High efficiency diesel engine with low heat loss combustion concept - Toyota's inline 4-cylinder 2.8-liter ESTEC 1GD-FTV Engine, SAE Technical Paper 2016-01-0658, 2016.

[20] J.B. Heywood, *Chapter 12, Engine heat transfer in "*Internal Combustion Engine Fundamentals", McGraw-Hill Inc, 1998.

[21] C. Rakopoulos, G. Mavropoulos, D. Hountalas, Measurements and analysis of load and speed effects on the instantaneous wall heat fluxes in a direct injection air-cooled diesel engine, Int. J. Energy Res. 24 (7) (2000) 587–604.

[22] J. Chang, O. Güralp, Z. Filipi, D. Assanis, et al., New heat transfer correlation for an HCCI engine derived from measurements of instantaneous surface heat flux, SAE Technical Paper 2004-01-2996, 2004.

[23] A. Kikusato, K. Terahata, K. Jin, Y. Daisho, A numerical simulation study on improving the thermal efficiency of a spark ignited engine—part 2: Predicting instantaneous combustion chamber wall temperatures, heat losses and knock—, SAE Int. J. Engines 7 (1) (2014) 87–95.

[24] C. Knappe, P. Andersson, M. Algotsson, M. Richter, J. Linden, M. Alden, M. Tuner, B. Johanson, Laser-induced phosphorescence and the impact of phosphor coating thickness on Crank-Angle Resolved Cylinder Wall temperatures, SAE Technical Paper 2011-01-1292, 2011.

[25] M. Algotsson, C. Knappe, M. Tunér, M. Richter, B. Johansson, M. Aldén, In-cylinder surface thermometry using laser induced phosphorescence. In The Eighth International Conference on Modeling and Diagnostics for Advanced Engine Systems (COMODIA 2012), pp. 482–487. Japan Society of Mechanical Engineers.

[26] Broatch, A., Olmeda, P., Margot, X., & Escalona, J. (2019). New approach to study the heat transfer in internal combustion engines by 3D modelling. International Journal of Thermal Sciences, 138, 405-415.

[27] Wallace, F. J., R. J. B. Way, and H. Vollmert. Effect of partial suppression of heat loss to coolant on the high output diesel engine cycle. No. 790823. SAE Technical Paper, 1979.

[28] A. Bejan, A.D. Kraus. *Basic Concepts* in "Heat transfer handbook". United States of America. John Wiley & Sons, 2003.

[29] Andruskiewicz, P., Najt, P., Durrett, R., & Payri, R. (2018). Assessing the capability of conventional in-cylinder insulation materials in achieving temperature swing engine performance benefits. International Journal of Engine Research, 19(6), 599–612. https://doi.org/10.1177/1468087417729254

[30] M. Lapuerta, O. Armas, J. Hernández, Diagnosis of DI diesel combustion from in-cylinder pressure signal by estimation of mean thermodynamic properties of the gas, Applied Thermal Engineering 19 (5) (1999) 513-529. doi:10.1016/S1359-4311(98)00075-1.

[31] F. Payri, S. Molina, J. Martín, O. Armas, Influence of measurement errors and estimated parameters on combustion diagnosis, Applied Thermal Engineering 26 (2) (2006) 226 – 236. doi:10.1016/j.applthermaleng.2005.05.006.

[32] A. J. Torregrosa, P. Olmeda, J. Martin, et al., A Tool for Predicting the Thermal Performance of a Diesel Engine, Heat Transfer Engineering, 2011, 32 (10):891-904.

[33] F. Payri, P. Olmeda, C. Guardiola, et ál., Adaptive determination of cut-off frequencies for filtering the in-cylinder pressure in diesel engines combustion analysis, Applied Thermal Engineering 14-15 (31), 2869-2876.

[34] F. Payri, P. Olmeda, J. Martín, A. García, A complete 0D thermodynamic predictive model for direct injection diesel engines Applied Energy 88 (2011) 4632–4641, doi:10.1016/j.apenergy.2011.06.005.

[35] Arrègle, J., López, J. Martín, J. Mocholí, E.M., Development of a Mixing and Combustion Zero-Dimensional Model for Diesel Engines, SAE Technical paper 2006-01-1382, 2006.

[36] Olmeda, P., Martín, J., Arnau, F. J., & Artham, S. Analysis of the energy balance during World harmonized Light vehicles Test Cycle in warmed and cold conditions using a Virtual Engine. International Journal of Engine Research, 1468087419878593, 2019.